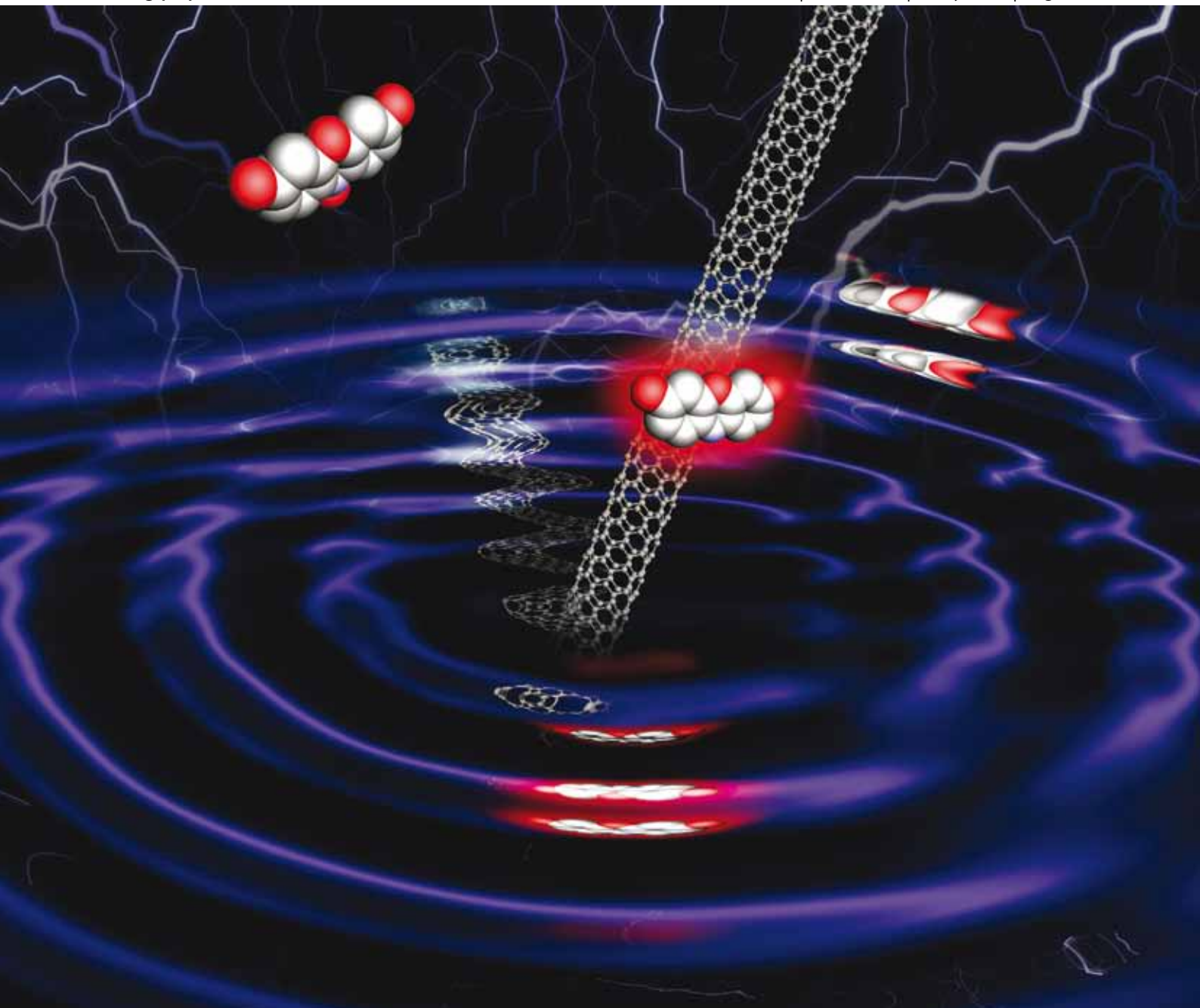


PCCP

Physical Chemistry Chemical Physics

www.rsc.org/pccp

Volume 12 | Number 25 | 7 July 2010 | Pages 6537–6876



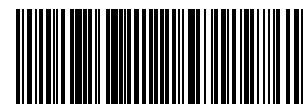
ISSN 1463-9076

COVER ARTICLE

Chen *et al.*
Single-molecule nanoscale
electrocatalysis

PERSPECTIVE

Leone *et al.*
Chemical dynamics, molecular
energetics, and kinetics at the
synchrotron



1463-9076(2010)12:25;1-Z

Single-molecule nanoscale electrocatalysis

Hao Shen, Weilin Xu† and Peng Chen*

Received 8th January 2010, Accepted 25th February 2010

First published as an Advance Article on the web 9th April 2010

DOI: 10.1039/c000448k

Nanoscale catalysts are important for electrocatalysis, especially in energy conversion as in photoelectrochemical cells and fuel cells. Understanding their reactivity is essential for improving their performances and designing new ones, but challenging due to their inherent structural heterogeneity. This article reviews recent developments in using single-molecule fluorescence microscopy to overcome this challenge and interrogate directly the individuality of nanoscale catalysts. Using electrocatalysis by single-walled carbon nanotubes (SWNTs) as an example, this article discusses how the single-molecule approach dissects the reaction kinetics at single-reaction resolution, unravels the reaction mechanism, and quantifies the reactivity and inhomogeneity of individual SWNT reactive sites, which are imaged to nanometre precision *via* super-resolution optical imaging. New scientific questions and opportunities are also discussed, as well as the related optical studies of single-molecule and single-nanoparticle electrochemistry.

1. Introduction

Catalysis at the nanoscale is a cornerstone technology for meeting the current energy challenge. Nanoscale catalysts of various materials can enable chemoselective processing of fossil fuels, remove pollutants from gas exhausts, increase fuel usage efficiency, and promote solar energy conversion to fuels.^{1–3} With the rapid advances in nanostructure synthesis, new nanoscale catalysts and novel catalytic properties continue to emerge.^{4,5}

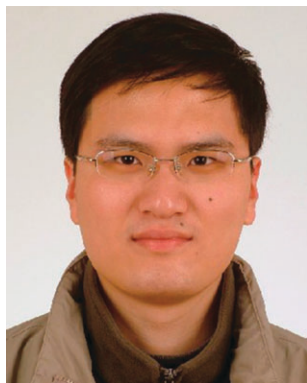
Often nanoscale catalysts are used on electrodes, where the catalysis takes place in the presence of an electrochemical potential and is coupled with electron flow, hence electrocatalysis. In photoelectrochemical cells, sunlight is collected and converted to electricity, which then drives chemical reactions to form fuels. In fuel cells, the fuels undergo redox reactions

to release their chemical energy to generate electricity. Both the fuel-forming and the fuel-using reactions need to be catalyzed, usually by nanoscale catalysts, to achieve sufficient efficiency and selectivity. Improving the performance of current catalysts and designing new ones are major goals in today's catalysis research. To achieve these goals, an essential task is to understand the fundamental structure–activity correlations of nanoscale materials for electrocatalysis, as well as for catalysis in general.

For almost all nanoscale catalysts, structural heterogeneity is a problem. Nanoparticle catalysts of metals, metal oxides, *etc.*, always have some structural dispersion, such as in size and shape; even on a single particle, surface atoms reside at various corner, edge, and facet sites.^{6,7} Nanotubes and nanowires, such as carbon nanotubes, have variable diameters and lengths, and along their lengths, various catalytic sites can be present.⁸ As structure dictates activity, individual nanocatalysts are expected to differ in their catalytic properties due to this structural heterogeneity.

This structural heterogeneity poses a general challenge in characterizing the catalytic properties of nanoscale materials.

Department of Chemistry and Chemical Biology, Cornell University, Ithaca, New York 14853, USA. E-mail: pc252@cornell.edu
† Current address: Department of Chemical Engineering, University of California, Berkeley, California 94720, USA.



Hao Shen

Hao Shen obtained his BS in Chemistry at Nanjing University, China in 2003. He is currently a graduate student in Prof. Peng Chen's group in the Department of Chemistry and Chemical Biology at Cornell University. His research is on single-molecule study of electrocatalysis by carbon nanotubes and other carbon-based materials.



Weilin Xu

Weilin Xu obtained his BS in chemistry at Jilin University, China in 2001, and his PhD at Changchun Institute of Applied Chemistry, Chinese Academy of Sciences in 2006. During 2007–2009, he was a postdoctoral fellow with Prof. Peng Chen at Cornell University, working on single-molecule catalysis of nanomaterials. He is currently a postdoctoral researcher in the Department of Chemical Engineering at University of California, Berkeley.

Traditional measurements, which analyze reaction products produced by an ensemble of nanocatalysts, often only obtain their averaged catalytic behaviors, where individuality is lost. Experimental methods capable of resolving the individual behaviors of nanocatalysts are thus highly desired.

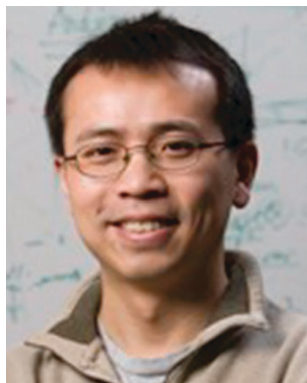
The single-molecule approach can directly probe individuality and is particularly suited for studying heterogeneous systems, including nanoscale catalysts. Besides removing ensemble averaging, it allows visualization of catalytic reactions in real time with single-turnover resolution, a feature that is powerful in dissecting reaction mechanisms. Moreover, single-molecule fluorescence detection can offer optical imaging beyond the diffraction-limited resolution—tens of nanometres resolution is achievable—giving high spatial information.⁹

Our group has recently developed single-molecule fluorescence microscopy methods to study nanoscale catalysts.^{10–16} In one case, we studied the catalysis of metal nanoparticles at single-particle, single-turnover resolution.^{10–15} In another, we studied the electrocatalysis of single-walled carbon nanotubes (SWNTs) at single reactive site, single-reaction resolution.¹⁶ Both metal nanoparticles and SWNTs have inherent structural heterogeneity. Our single-molecule approaches enabled us to probe their individuality, quantify their reactivity, understand their mechanism, and discover new catalytic behaviors that are fundamental to nanoscale catalysis.

In this perspective, we focus the discussions on our single-molecule study of SWNT electrocatalysis. We review the methodology, the results, and the information content, as well as discuss the new scientific questions and opportunities that arise from our studies. We also summarize past single-molecule and single-nanoparticle electrochemistry studies that our work is closely related to.

2. Single-molecule fluorescence approach to nanoscale electrocatalysis

Our single-molecule study of nanoscale electrocatalysis started with SWNTs, which can electrocatalyze reactions that are of



Peng Chen

Peng Chen received his BS from Nanjing University, China in 1997. After a year at University of California, San Diego with Prof. Yitzhak Tor, he moved to Stanford University and did his PhD with Prof. Edward Solomon in bioinorganic/physical inorganic chemistry. In 2004, he joined Prof. Sunney Xie's group at Harvard University for postdoctoral research in single-molecule biophysics. He started his assistant professorship at Cornell

University in 2005. His current research focuses on single-molecule imaging of nanocatalysis and bioinorganic chemistry. He has received a Dreyfus New Faculty award, a NSF Career award, a Sloan Fellowship, and a Paul Saltman Award.

interest for energy applications,¹⁷ for example the oxygen reduction reaction.¹⁸ Structurally, a SWNT can be viewed as a graphene sheet rolled into a tube along a chiral vector, which is a linear combination of the two lattice vectors of the graphene honeycomb structure. Depending on this chiral vector (*i.e.*, its chirality), a SWNT can have different electronic properties, being either metallic or semiconducting.

Current preparation methods always produce SWNTs of variable chirality and thus of variable electronic property. Obtaining monodisperse SWNTs remains a persistent challenge. These chirality and electronic property variations can give individual nanotubes different electrochemical and electrocatalytic properties. To circumvent this polydispersion obstacle, people have studied the electrochemistry of individual carbon nanotubes, where the electrochemical current through a single nanotube is measured.^{19–21}

For electrocatalysis studies, measuring electrical currents, although informative, cannot differentiate where the electrocatalysis takes place on the nanotube. Yet, differentiating reactions spatially is important, as recent studies have shown that defect sites or exogenous atoms may be the origin of special catalytic activity of carbon nanotubes.^{18,22–25} Furthermore, electrical current measurements typically can only be performed on one nanotube at a time, limiting the data throughput. To increase data throughput, multiplexed observations of electrochemistry or electrocatalysis by carbon nanotubes are needed.

Our group has recently developed a single-molecule fluorescence approach to study SWNT electrocatalysis in a multiplexed manner at single-reaction temporal resolution and nanometre spatial precision.¹⁶ Fig. 1a depicts our experimental design using an electrochemical flow cell, which is similar to that by Barbara and Bard in their single-molecule spectroelectrochemistry studies (section 4.1),^{26,27} and total internal reflection fluorescence microscopy. We disperse well-sonicated, diluted SWNT suspensions onto an ITO-coated quartz slide, so individual SWNTs are spatially well separated. The conductive ITO surface serves as the working electrode. We also place a Ag/AgCl reference electrode and a Pt counter electrode in the flow cell. Above the working electrode, we flow a solution containing a reactant that can be electrocatalytically converted by SWNTs into a fluorescent product. Each electrocatalytic reaction generates a fluorescent molecule; under CW laser illumination, this fluorescent molecule emits hundreds or more fluorescence photons and is readily detectable at the single-molecule level. By detecting every product molecule, we can visualize the electrocatalysis at the single-reaction resolution in real time. This fluorogenic reaction strategy was started in single-enzyme studies^{28–31} and has also been employed in studying micro- and nano-scale solid catalysts.^{32,33}

In this experimental scheme, the applied electrochemical potential on the ITO working electrode can effectively change the chemical potential of SWNTs due to the nanotubes' small quantum capacitances.^{20,21,34} This scheme also has a number of advantageous features. (1) A continuous solution flow and a constant applied electrochemical potential can ensure steady-state reaction

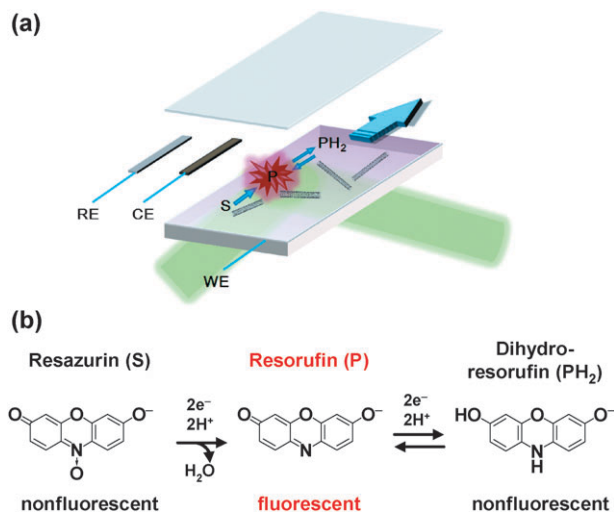


Fig. 1 Single-molecule fluorescence approach to carbon nanotube electrocatalysis. (a) Experimental design using an electrochemical flow cell made between an ITO-coated quartz slide and a coverslip, and total internal reflection fluorescence microscopy. WE, RE, CE: working, reference, and counter electrodes. (b) Redox chemistry of resazurin in aqueous solution. Figures adapted with permission from Xu *et al.*¹⁶ Copyright 2009 American Chemical Society.

conditions and easy change of the reactant concentration. (2) Because the products are continuously generated, such experiments can monitor electrocatalytic reactions of a SWNT for extended time without the limit of fluorescence photobleaching. (3) The wide-field imaging allows multiplexed observation of many SWNTs. (4) The single-molecule detection enables imaging the electrocatalytic reactions at nanometre resolution to differentiate reactions occurring at different locations (section 3.2).

Our fluorogenic electrocatalytic reaction is based on the well-known two-stage electro-reduction of the nonfluorescent molecule resazurin in aqueous solution (Fig. 1b).³⁵ The first stage reduces resazurin (S) irreversibly to resorufin (P), a highly fluorescent molecule. The second stage reduces resorufin to the nonfluorescent dihydroresorufin (PH₂) and is reversible. The fluorescence of P is the target of our single-molecule detection and can be excited by a 532-nm laser. Ensemble cyclic voltammetry clearly demonstrates the ability of SWNTs in electrocatalyzing the two-stage reduction of S and that the electrocatalysis happens to SWNT surface adsorbed molecules.¹⁶ Control experiments also show that the observed electrocatalytic reactivity is not due to possible residual metal nanoparticle catalysts, amorphous carbons, or carbon nanoparticles in the SWNT sample.¹⁶

In the next section, we discuss the single-molecule measurements of SWNT electrocatalysis based on this electrocatalytic fluorogenic reaction, the physical nature of the reactive sites on the SWNTs, and the reactivity and mechanism of the electrocatalysis. We also discuss new scientific questions and opportunities that arise from these results, as well as limitations in the single-molecule approach to nanoscale electrocatalysis.

3. Application to carbon nanotube electrocatalysis

3.1 Real-time single-molecule detection of SWNT electrocatalysis

We studied SWNTs either obtained commercially (Purified HiPCO, from Carbon Nanotechnologies) or home-grown *via* the CVD method. Upon applying a constant electrochemical potential to the ITO electrode in the flow cell (Fig. 1a), electrocatalysis occurs on SWNTs and generates fluorescent P molecules. Imaged by an EMCCD camera with single-molecule sensitivity, the electrocatalysis gives out stochastic fluorescence bursts at many localized spots on the ITO working electrode. A typical fluorescence image from a real-time movie contains many fluorescence spots of diffraction limited size (FWHM \sim 400 nm, Fig. 2a).

At these localized spots, the fluorescence bursts occur *repetitively*. This repetitiveness is manifested in the time trajectory of fluorescence intensity from one of these spots (Fig. 2b): it contains stochastic off-on burst signals throughout the movie. The digital, two-state nature of these fluorescence trajectories verifies the single-molecule detection of the electrocatalysis, in which each burst comes from a single P molecule. Were it from many molecules, the trajectory would have variable number of intensity states depending on the number of molecules. This single-molecule detection enables us to probe the nature of the reactive sites, as well as the reactivity and mechanism of electrocatalysis at an unprecedented level (see below).

3.2 Super-resolution optical imaging of SWNT reactive sites

SWNTs are 1-dimensional nanomaterials. The diameters of the SWNTs studied here are about 1–2 nm, but their lengths

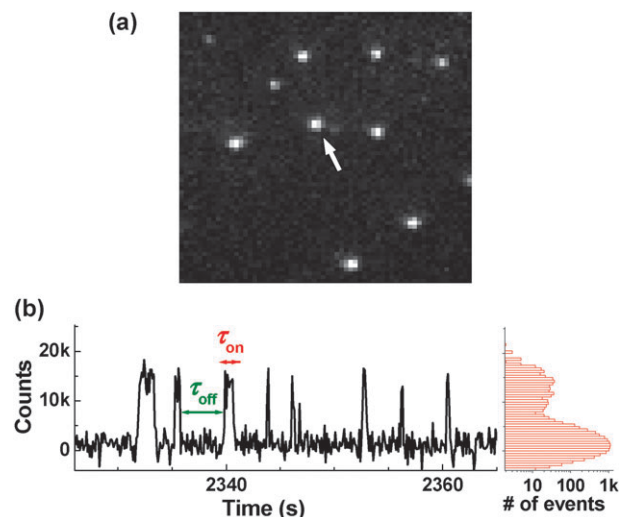


Fig. 2 Real-time single-molecule fluorescence detection of SWNT electrocatalysis. (a) Fluorescence image ($\sim 17 \times 19 \mu\text{m}^2$) of SWNT electrocatalysis at -0.35 V with $0.05 \mu\text{M}$ resazurin (S) in phosphate buffer. Taken at 100-ms frame rate. All potentials cited here are referenced to the Ag/AgCl electrode. (b) Left: segment of the fluorescence trajectory from the fluorescence spot marked by the arrow in (a). Right: histogram of an 18-minute long trajectory. Figures adapted with permission from Xu *et al.*¹⁶ Copyright 2009 American Chemical Society.

can be many microns.³⁶ Electrocatalysis can potentially occur at various sites on a SWNT: the honey-comb structured sidewall, the ends of the nanotube, or defect sites that can reside anywhere along the sidewall. To probe where the reactions take place is one of the first steps toward understanding the electrocatalytic properties of SWNTs.

Structurally, the sidewall of a SWNT is continuous, whereas its ends and defect sites are discrete. In the fluorescence image (Fig. 2a), the localization of the fluorescence bursts within diffraction-limited spots suggests that the reactions occur at discrete sites (*e.g.*, defect sites or nanotube ends), rather than on the entire nanotube sidewall. Higher spatial resolution is needed, however, beyond the diffraction limit to confirm the discreteness of these reactive sites, as the diameters of these SWNTs are merely 1–2 nm.

Single-molecule fluorescence detection enables just that, *via* the so-called super-resolution optical imaging method,^{9,37–39} as in photoactivation localization microscopy (PALM)^{37,39} and stochastic optical reconstruction microscopy (STORM).^{38,40–42} These super-resolution microscopy techniques use two features of single-molecule fluorescence detection to achieve sub-diffraction resolution. The first is the nanometre accuracy in localizing the center of the emission point spread function (PSF) of a single fluorescent molecule in a wide-field image, provided that a large number of fluorescence photons are detected (the localization accuracy is approximately proportional to $1/\sqrt{\text{number of photons detected}}$).^{43,44} Fig. 3a shows the wide-field fluorescence image of a single **P** molecule at a SWNT reactive site; the fluorescence intensity spreads over a few pixels as a PSF (each pixel = 267 nm). Because of the large number of photons detected, fitting this PSF with a two-dimensional Gaussian function localizes its center position to about ± 4.5 nm accuracy (Fig. 3b), even though the FWHM of this PSF is ~ 410 nm.

The second feature is the temporal separation of fluorescence detection of individual molecules that reside within the diffraction-limited resolution (\sim a few hundred nanometres). This temporal separation is manifested by the off–on signals in the fluorescence intensity trajectories and can be achieved through photo-induced switching of fluorescent molecules as in PALM and STORM, or, as in the SWNT electrocatalysis done here, through electrocatalytic generation of individual fluorescent **P** molecules (Fig. 2b). Consequently, the localizations of the many **P** molecules in a fluorescence trajectory can be determined individually, each down to an accuracy of a few nanometres.

The localizations of these **P** molecules show a spread and follow a Gaussian distribution (Fig. 3c).^{38,41,42} The FWHM of the localization distribution gives the spatial resolution of ~ 20 nm (Fig. 3d), comparable to those in PALM and STORM^{37–39,41,42} and an order of magnitude higher than the resolution (~ 400 nm) in the diffraction-limited wide-field fluorescence image (Fig. 3a). Considering the diameters of these SWNTs are about 1–2 nm,³⁶ these reactive sites should thus be no more than $\sim 2 \times 20$ nm² in dimension. Although without experimental proof, we think these reactive sites are probably smaller than our resolution, *i.e.*, at about the molecular scale.

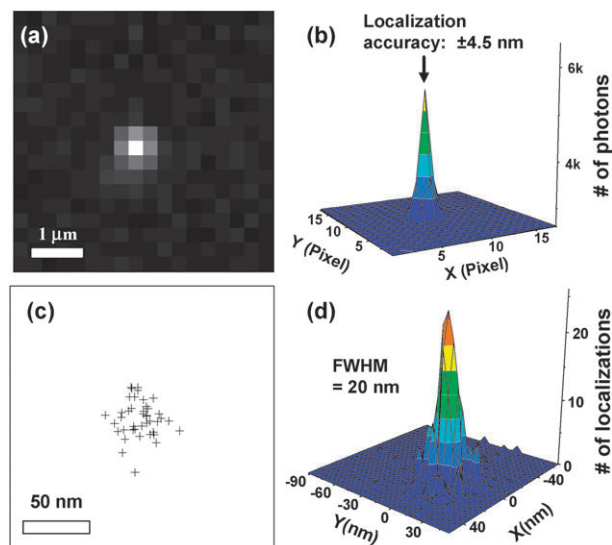


Fig. 3 Super-resolution optical microscopy of SWNT reactive sites. (a) Conventional wide-field fluorescence image of a single resorufin (**P**) at a reactive site during one τ_{on} period. Pixel size = 267 nm. (b) Two-dimensional Gaussian fit to the PSF function in (a). The FWHM of the fit is ~ 410 nm. The center localization is determined to ± 4.5 nm. (c) Center localizations determined from the many τ_{on} periods of a fluorescence electrocatalysis trajectory. (d) Two-dimensional histogram of the center localizations. Gaussian fit gives FWHM ~ 20 nm. To increase statistics, the localizations from 25 reactive sites are combined, and the center of mass of the localizations from each reactive site was used for alignment. Figures adapted with permission from Xu *et al.*¹⁶ Copyright 2009 American Chemical Society.

The nanometre dimension of these reactive sites offers a distinctive advantage: Each reactive site on a SWNT acts as an ultrasmall electrode, for which the mass transport is efficient,⁴⁵ thus allowing the study of electrocatalytic electron-transfer kinetics at low reactant concentrations (see section 3.5).

3.3 Kinetic mechanism of electrocatalysis

In the fluorescence electrocatalysis trajectory of a single SWNT reactive site (Fig. 2b), the actual events of chemical transformations are irresolvable and appear as sudden intensity jumps. Each sudden intensity increase corresponds to an electrocatalytic formation of a single **P** molecule at a reactive site. The sudden intensity decreases primarily result from electro-reduction events of **P** to **PH₂**—other possible causes, such as **P** photobleaching, photoblinking, and dissociation from a SWNT, all happen at much slower time-scales (seconds to tens of seconds) and do not contribute significantly to these sudden intensity decreases.¹⁶

The waiting times, τ_{on} and τ_{off} , before the intensity jumps are the two most important observables in these trajectories (Fig. 2b). Resolving them temporally enables the analysis of the electrocatalysis kinetics in two separate parts: τ_{on} is the waiting time for electro-reduction of **P** to **PH₂** after a **P** molecule is formed at a reactive site; τ_{off} is the waiting time for **P** formation and contains binding of **S** to the reactive site from the solution. The individual values of τ_{on} and τ_{off} are stochastic, but their statistical properties, such as average

values and distributions, are defined by the reaction kinetics and thus report the kinetic mechanism.

At constant electrochemical potentials, the electro-reduction of **P** to **PH₂** contained in τ_{on} follows a simple, one step **P** \rightarrow **PH₂** reaction kinetics (reaction (iv), Fig. 4a). This simple kinetic mechanism of **P** electro-reduction is manifested experimentally by the **S** concentration ($[\text{S}]$) titration of $\langle\tau_{\text{on}}\rangle^{-1}$ ($\langle\ \rangle$ denotes averaging), which represents the time-averaged **P** reduction rate at a single reactive site. Regardless of the applied electrochemical potential, $\langle\tau_{\text{on}}\rangle^{-1}$ is independent of $[\text{S}]$ (Fig. 4b). This behavior of $\langle\tau_{\text{on}}\rangle^{-1}$ is quantitatively described by the following equation:

$$\langle\tau_{\text{on}}\rangle^{-1} = 1/\int_0^\infty \tau f_{\text{on}}(\tau) d\tau = k_4^{\text{red}} \quad (1)$$

where $f_{\text{on}}(\tau)$ is the probability density function of τ_{on} , and k_4^{red} is the rate constant of **P** \rightarrow **PH₂** electro-reduction at a single SWNT reactive site. Being the rate constant of an electro-reduction reaction, k_4^{red} , and thus $\langle\tau_{\text{on}}\rangle^{-1}$, are dependent on the electrical potential and increase with more negative potential (Fig. 4b).

For the electrocatalytic formation of **P** contained in τ_{off} , the reaction kinetics contains two parallel reaction pathways. One involves a substitution reaction of **PH₂** by **S** at the reactive site followed by electrocatalytic reduction of **S** to **P** (reactions (i) and (ii), Fig. 4a), the other is a direct electro-oxidation of **PH₂** to **P** (reaction (iii)). This electro-oxidation is possible because

P \leftrightarrow **PH₂** redox is reversible (Fig. 1b). This two-pathway kinetics of the τ_{off} reaction is manifested by the variable $[\text{S}]$ dependence of $\langle\tau_{\text{off}}\rangle^{-1}$, the time-averaged rate of **P** formation at a single reactive site (Fig. 4c): at more negative potentials (e.g., at -0.35 V), $\langle\tau_{\text{off}}\rangle^{-1}$ increases asymptotically with increasing $[\text{S}]$; at less negative potentials (e.g., at -0.1 V), $\langle\tau_{\text{off}}\rangle^{-1}$ decreases asymptotically. This variable $[\text{S}]$ dependence of $\langle\tau_{\text{off}}\rangle^{-1}$ is described quantitatively by the following equation:

$$\langle\tau_{\text{off}}\rangle^{-1} = 1/\int_0^\infty \tau f_{\text{off}}(\tau) d\tau = \frac{k_2^{\text{red}}(k_3^{\text{ox}} + k_1[\text{S}])}{k_2^{\text{red}} + k_1[\text{S}]} \quad (2)$$

where $f_{\text{off}}(\tau)$ is the probability density function of τ_{off} , k_1 is the rate constant of **PH₂** substitution by **S** at the reactive site (reaction (i)), k_2^{red} is the rate constant of electro-reduction of **S** to **P** (reaction (ii)), and k_3^{ox} is the rate constant of electro-oxidation of **PH₂** to **P** (reaction (iii)). At $[\text{S}] \rightarrow 0$, $\langle\tau_{\text{off}}\rangle^{-1} = k_3^{\text{ox}}$; at $[\text{S}] \rightarrow \infty$, $\langle\tau_{\text{off}}\rangle^{-1} = k_2^{\text{red}}$. As k_3^{ox} is an electro-oxidation reaction and k_2^{red} is an electro-reduction reaction, both of them depend on the applied electrochemical potential, but in opposite trends— at more negative potentials, electro-reduction is more favorable, and $k_3^{\text{ox}} < k_2^{\text{red}}$; at less negative potentials, electro-oxidation is more favorable, and $k_3^{\text{ox}} > k_2^{\text{red}}$. Therefore, when the electrochemical potential changes, $\langle\tau_{\text{off}}\rangle^{-1}$ shows different $[\text{S}]$ dependences, depending on the relative magnitudes of k_3^{ox} and k_2^{red} (Fig. 4c).

3.4 Reactivity inhomogeneity among SWNT reactive sites

Due to chirality differences, individual SWNTs can have different electrocatalytic properties, causing them to show different electrocatalytic reactivity. But, how different are they? Are the differences significant? Their reactivity differences, *i.e.*, reactivity inhomogeneity, are extremely difficult to quantify in ensemble-averaged measurements, but can be directly examined and quantified in the single-molecule measurements of single reactive sites. At any applied electrochemical potential for each reactive site, we can examine the $[\text{S}]$ dependences of its $\langle\tau_{\text{on}}\rangle^{-1}$ and $\langle\tau_{\text{off}}\rangle^{-1}$ (Fig. 5a). Fitting these two $[\text{S}]$ titration curves with eqn (1) and (2) directly gives the kinetic constants k_1 , k_2^{red} , k_3^{ox} , and k_4^{red} , which quantify the reactivity of this reactive site.

Alternatively, we can examine the distributions of τ_{on} and τ_{off} from the fluorescence electrocatalysis trajectory of a single reactive site. Regardless of $[\text{S}]$, the probability density function of τ_{on} , $f_{\text{on}}(\tau)$, follows $f_{\text{on}}(\tau) = k_4^{\text{red}} \exp(-k_4^{\text{red}}\tau)$.¹⁶ For the probability density function of τ_{off} , $f_{\text{off}}(\tau)$, it reduces to $f_{\text{off}}(\tau) = k_2^{\text{red}} \exp(-k_2^{\text{red}}\tau)$ at saturating resazurin concentrations (*i.e.*, $[\text{S}] > 0.1$ μM for the SWNTs studied here).¹⁶ Therefore, k_4^{red} and k_2^{red} of a reactive site can be directly determined by fitting its distributions of τ_{on} and τ_{off} with exponential functions (Fig. 5b).

By analyzing many fluorescence electrocatalysis trajectories, we can obtain the distributions of kinetic rate constants among many SWNT reactive sites at any applied potential, for example those of k_2^{red} and k_4^{red} in Fig. 5c. As expected, their distributions are dependent on the applied potential. Relative to their average values, the distribution widths of all rate constants are broad, indicating the large reactivity inhomogeneity among the SWNT reactive sites. Several of these rate

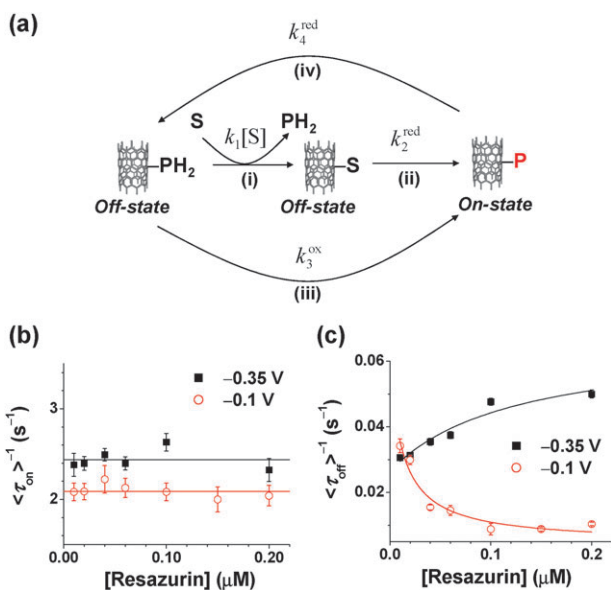


Fig. 4 Kinetic mechanism of SWNT electrocatalysis. (a) Scheme of the kinetic mechanism. The fluorescence state (on or off) is indicated at each stage of the reaction. **S**, resazurin; **P**, resorufin; **PH₂**, dihydroresorufin. (b, c) Resazurin concentration dependence of $\langle\tau_{\text{on}}\rangle^{-1}$ and $\langle\tau_{\text{off}}\rangle^{-1}$ at two different potentials. Data here are averaged over the fluorescence trajectories of > 50 reactive sites. Solid lines are fits of eqn (1) and (2); for -0.35 V, $k_1 = 0.5$ $\mu\text{M}^{-1}\text{s}^{-1}$, $k_2^{\text{red}} = 0.07$ s^{-1} , $k_3^{\text{ox}} = 0.026$ s^{-1} , $k_4^{\text{red}} = 2.4$ s^{-1} ; for -0.1 V, $k_1 = 0.3$ $\mu\text{M}^{-1}\text{s}^{-1}$, $k_2^{\text{red}} = 0.004$ s^{-1} , $k_3^{\text{ox}} = 0.06$ s^{-1} , $k_4^{\text{red}} = 2.1$ s^{-1} . Note the values here represent the averaged properties of many SWNT reactive sites. Figures adapted with permission from Xu *et al.*¹⁶ Copyright 2009 American Chemical Society.

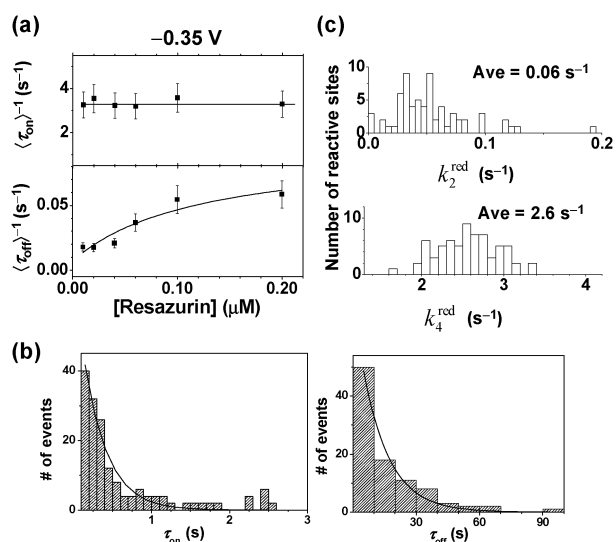


Fig. 5 Reactivity inhomogeneity of SWNT reactive sites. (a) Resazurin concentration ($[S]$) dependence of $\langle \tau_{\text{on}} \rangle^{-1}$ and $\langle \tau_{\text{off}} \rangle^{-1}$ of a single reactive site at -0.35 V. Solid lines are fits with eqn (1) and (2) with $k_1 = 0.8 \pm 0.6 \mu\text{M}^{-1} \text{s}^{-1}$, $k_2^{\text{red}} = 0.09 \pm 0.04 \text{s}^{-1}$, $k_3^{\text{ox}} = 0.01 \pm 0.01 \text{s}^{-1}$, $k_4^{\text{red}} = 3.3 \pm 0.1 \text{s}^{-1}$. (b) Distributions of τ_{on} and τ_{off} , each from the fluorescence electrocatalysis trajectory of a SWNT reactive site at the saturating resazurin concentration of $0.2 \mu\text{M}$. Solid lines are exponential fits, giving $k_4^{\text{red}} = 3.4 \pm 0.1 \text{s}^{-1}$ and $k_2^{\text{red}} = 0.08 \pm 0.01 \text{s}^{-1}$, respectively. (c) Distributions of k_2^{red} and k_4^{red} from many SWNT reactive sites at -0.35 V. Figures (a,c) adapted with permission from Xu *et al.*¹⁶ Copyright 2009 American Chemical Society.

constants, such as k_2^{red} and k_4^{red} , involve interfacial electron transfer from a SWNT to an adsorbed molecule and are thus related to the electronic properties of the SWNT reactive sites. Therefore, the broad distributions of these rate constants reflect the variable electronic properties among these discrete reactive sites, which could come from the different chemical nature of these sites, or from the different electronic properties of SWNTs (*e.g.*, metallic or semiconducting).

Nevertheless, as the SWNTs are deposited on the ITO surface nonspecifically (Fig. 1a), we could not rule out that variations in the electrical contact between a SWNT and the ITO may also contribute to the observed reactivity inhomogeneity. Future experiments using metal electrodes evaporated directly onto the SWNTs will help minimize contact variability.²⁰

3.5 New questions, new opportunities, and limitations

As described in sections 3.1–3.4, single-molecule fluorescence microscopy of SWNT electrocatalysis offers insights into the physical nature of the reactive sites, the kinetic mechanism of the reaction, the reactivity of each reactive site, and the variations of catalytic properties among the SWNT reactive sites, much of which are unavailable from traditional ensemble measurements or single-nanotube electrochemical current measurements. With this new information, new questions also arise. For example, what is the chemical nature of the catalytic reactive sites on the SWNTs, *i.e.*, what are the functional groups at the reactive sites? The possibilities include carboxylate,

carbonyl, and hydroxo groups.^{46,47} To probe these functional groups, one can target them with chemoselective reagents and then examine their effects on the SWNTs' electrocatalytic activity. An example is to use an esterification reaction to modify carboxylate groups selectively.

Super-resolution optical imaging has shown that the SWNT reactive sites are discrete and are of nanometres in dimension. But, where are they exactly located on a SWNT? At the ends of the nanotube or scattered on the sidewall? Parallel measurements using atomic force microscopy (AFM) or scanning electron microscopy (SEM) will provide definitive answers. For this purpose, the nanometre resolution of super-resolution optical imaging facilitates the image correlation between fluorescence microscopy and AFM/SEM—this correlation is usually hampered by the resolution mismatch in the respective measurements, with traditional fluorescence microscopy having half-a-micron resolution whereas AFM/SEM having nanometre resolution.

The location of reactive sites on a SWNT brings up another intriguing question: do different sites on the same nanotube have the same electrocatalytic reactivity? Or do they differ significantly? Correlating AFM/SEM imaging with our single-molecule imaging of SWNT electrocatalysis will be able to address this question. The results will reveal whether the nature of the reactive site or the electronic property of the nanotube determines its electrocatalytic reactivity.

If the electronic property of a SWNT plays an important role, then how is a nanotube's electronic property correlated with its electrocatalytic reactivity? Independent determination of the electronic properties of a SWNT is needed here, in addition to the electrocatalysis study. Many methods already exist to determine the electronic property of a SWNT, such as electron transport measurements and Rayleigh scattering spectroscopies.^{48–50}

New scientific opportunities also arise from our ability to image SWNT electrocatalysis at single-reaction, single reactive-site resolution. To start with, we can examine interfacial electron transfer involved in the electrocatalysis. Understanding electron transfer kinetics at solid-liquid interfaces is a key goal of basic research for energy production, conversion, and storage.⁵¹ In the SWNT electrocatalysis described here, both the τ_{on} and τ_{off} reactions involve interfacial electron transfer from a SWNT to a bound molecule sitting at the SWNT–solution interface (Fig. 4a). For example, the τ_{on} reaction is a single step electro-reduction reaction, $\text{P} \rightarrow \text{PH}_2$, with $\langle \tau_{\text{on}} \rangle^{-1}$ equal to k_4^{red} , the rate constant of this reaction. By studying the electrocatalysis across a range of applied electrochemical potentials, we can then study how the electrochemical driving force changes the interfacial electron transfer kinetics.

Fig. 6 shows our preliminary result of electrochemical potential titration of $\langle \tau_{\text{on}} \rangle^{-1}$ of a single SWNT reactive site. With increasingly negative potential, *i.e.*, increasing driving force for electro-reduction, $\langle \tau_{\text{on}} \rangle^{-1}$ increases and eventually saturates. This behavior is consistent with the theoretical simulations of the interfacial electron transfer kinetics for an electro-reduction reaction on a SWNT.²¹ Quantitative analysis of this type of data using the Gerischer–Marcus model can provide fundamental knowledge on the electronic coupling

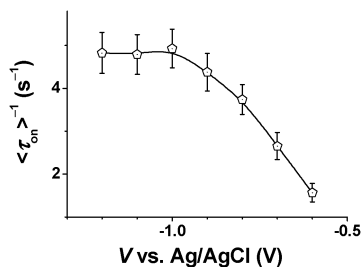


Fig. 6 Potential (V) dependence of $\langle \tau_{on} \rangle^{-1}$ of a SWNT reactive site at $[S] = 0.06 \mu\text{M}$. Each data point is an average of the many τ_{on} values in the fluorescence electrocatalysis trajectory at the corresponding applied electrochemical potential. The solid line is a B-spline that helps visualize the trend.

between the nanotube and the molecule, the reorganization energy, and the optimal rate for interfacial electron transfer.^{21,51–53}

Moreover, both metallic nanotubes and semiconducting ones are present in any SWNT sample; and for the semiconducting ones, individual SWNTs can have different bandgaps. In our multiplexed observation of SWNT electrocatalysis, we will then be able to study how the electronic structure of a SWNT affects the interfacial electron transfer process. This is of particular interest for semiconducting SWNTs, as they show promise as a next generation photovoltaics due to their good conductivity, broad absorption spectra, tunable bandgap, and capability in multi-exciton generation.^{54–56}

The single-molecule approach to nanoscale electrocatalysis does not come without limitations. The detection requires a fluorescent product, and as such, electrocatalysis involving merely small molecules, such as proton reduction to H_2 , cannot be studied *directly*. The types of electrocatalytic transformations are not limited, however, because one can create reactant molecules that undergo the desired transformation to generate a fluorescent molecule. For example, if electro-oxidation of alcohols to ketones is of interest, one can design a molecule that if oxidized, the resulted $\text{C}=\text{O}$ double bond completes an extended conjugation, forming a fluorescent product. The P to PH_2 electro-reduction discussed in this article is another example: it contains both electron and proton transfer processes, comprising two electrons and two protons, which is fundamentally related to the proton reduction reaction for fuel generation.

Although powerful in dissecting kinetic mechanisms of reactions, single-molecule fluorescence measurements are less capable of determining molecular mechanisms, *i.e.*, how chemical bonds are broken and made in converting reactants to products. This is partly because of their limited time resolution, μs at best, whereas actual chemical transformations occur at a sub-picosecond timescale. Another reason is the limited chemical information contained in fluorescence about molecules. Complementary measurements, such as vibrational spectroscopy, are needed.

4. Related optical studies of single-molecule and single-nanoparticle electrochemistry

A number of electrochemical studies of single molecules and single nanoparticles exist in the literature, to which our

single-molecule nanoscale electrocatalysis work is related. Based on their detection methods, these studies can be divided into two types: one type uses optical detection and measures photon emission that results from electrochemical reactions; the other detects electrochemical current. Detection of current is a much more widely used method, for which we refer the readers to the recent review articles^{57–59} and references cited there for details.

In this section, we summarize the optical studies of electrochemistry of single molecules and single nanoparticles. These optical studies use two experimental schemes: laser-induced fluorescence (or luminescence) and electrogenerated chemiluminescence (ECL). A perspective article by Bard also discusses these studies.⁵⁸

4.1 Fluorescence detection

Barbara, Bard, and coworkers pioneered the method of single-molecule spectroelectrochemistry (SMS-EC) and used it to study the redox events of single molecules of the organic polymer poly(9,9-dioctylfluorene-*co*-benzothiadiazole) (F8BT), which is intrinsically fluorescent.^{26,27} They used an electrochemical cell (Fig. 7a) and immobilized individual polymer molecules on the ITO-working electrode. Scanning the electrochemical potential induces the electrochemical oxidation of these polymer molecules, leading to their fluorescence disappearance. By imaging the fluorescence with wide-field TIR fluorescence microscopy, they followed both the irreversible and the reversible oxidations of these molecules. In correlation with the applied potential, statistical analysis of these single-molecule events offered insights into the energetics and dynamics of charging traps in these polymeric materials that are important for solar cells.

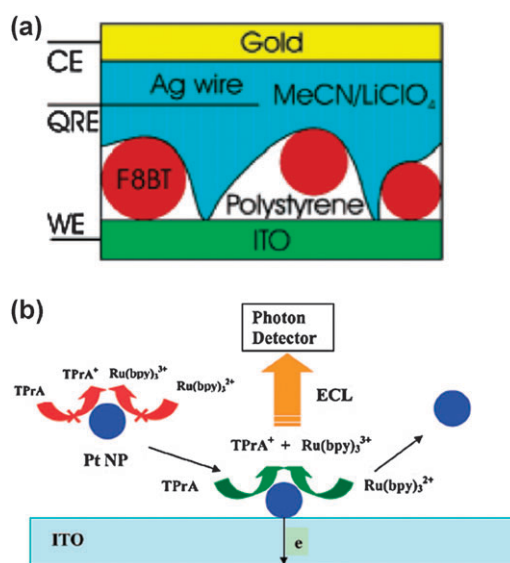


Fig. 7 (a) Electrochemical cell configuration from Barbara, Bard and coworkers. WE, CE, QRE: working, counter, and quasi-reference electrodes. Reproduced with permission from Palacios *et al.*²⁶ Copyright 2006 American Chemical Society. (b) Scheme of electrogenerated chemiluminescence amplification of single nanoparticle collisions. Reproduced with permission from Fan *et al.*⁶³ Copyright 2008 American Chemical Society.

Ackerman and coworkers extended the SMS-EC approach to a small electroactive molecule, cresyl violet, which is fluorescent in its oxidized form and nonfluorescent in its reduced form.^{60,61} In one study,⁶⁰ they used confocal fluorescence microscopy to detect in solution the fluorescent, oxidized cresyl violet molecules, whose population can be modulated by scanning the electrochemical potential. In another,⁶¹ they observed the reversible redox of single cresyl violet molecules adsorbed on clay nanoparticles, reflected by their fluorescence off-on behaviors under cyclic potential sweeping. Majima and coworkers also applied SMS-EC to study how the photoluminescence of single titania nanowires are affected by the applied electrochemical potentials.⁶²

4.2 Electrogenerated chemiluminescence

Wightman and coworkers first used ECL to detect electrochemical reactions of single molecules in solution.⁶⁴ They varied electrochemical potentials at an electrode to generate radical cations and anions of 9,10-diphenylanthracene (DPA) in solution; a cation and an anion then react to form an excited singlet state of DPA that can emit a photon to relax to the ground state. Detecting this photon emission allowed them to observe single molecule reactions.

Similarly, Barbara, Bard, and coworkers studied ECL of single F8BT polymer molecules using an SMS-EC cell as in Fig. 7a.⁶⁵ Here an immobilized, electrogenerated F8BT cation radical reacts with an electrogenerated radical of tri-*n*-propylamine (TPrA) in solution; the resulted excited state of F8BT then emits a photon that can be detected.

Bard and coworkers further broadened the ECL detection to observe single Pt nanoparticle collisions with an ITO electrode.⁶³ In their experiment (Fig. 7b), a collision event establishes an electrical contact between a Pt nanoparticle and the ITO-working electrode that is at a positive potential. This triggers electrochemical oxidations of Ru(bpy)₃²⁺ and TPrA on this Pt nanoparticle, and the oxidation products then react quickly to produce excited Ru(bpy)₃²⁺ molecules that emit photons for detection.

Compared with fluorescence detection, ECL does not involve laser excitation and thus has much less background signal. Yet one chemiluminescence reaction can maximally generate one photon (if the chemiluminescence has a quantum yield of 100%). As the efficiency of photon detection is far below 100%, many reactions go undetected. This does not prevent the study of single F8BT molecules, though, because each F8BT molecule can undergo repetitive ECL reactions to generate many photons, which ensures the detection of every F8BT molecule. For the study of Pt nanoparticle collisions, each collision triggers many ECL reactions, producing many photons and amplifying each collision event.

5. Concluding remarks

We have discussed the single-molecule fluorescence approach to nanoscale electrocatalysis, using carbon nanotube electrocatalysis as an example. By detecting the reaction products one molecule at a time in real time, this approach overcomes the inherent structural heterogeneity of nanoscale catalysts to probe their electrocatalytic individuality, resolve their discrete

reactive sites, dissect their reaction mechanism, and quantify their reactivity inhomogeneity. Much of these are beyond the reach of ensemble measurements or single-nanotube current measurements. Opportunities also arise to examine the correlation between the electronic structure, the electrocatalytic reactivity, and the interfacial electron transfer kinetics of nanoscale catalysts at the single reactive-site level.

The single-molecule fluorescence approach is generalizable for studying many other types of electrocatalysts of both nano- and macro-scale, including small molecule catalysts. So long as suitable fluorogenic reactions are available, real-time visualization of electrocatalytic reactions at single-reaction temporal resolution, nanometre spatial precision is feasible. With single-molecule studies continuing to emerge, new and deeper insights will be learned into the fundamental properties of nanoscale catalysts.

Acknowledgements

We thank Jiwoong Park and Yoon Ji Kim for collaboration, Xiaochun Zhou and Guokun Liu for contributing to the work discussed here, and Eric Choudhary and Weilin Meng for careful reading of the manuscript. We also thank the financial support from the Army Research Office (56355-CH), National Science Foundation (CBET-0851257), NSF-funded Cornell Center for Materials Research, and Alfred P. Sloan Research Fellowship.

References

- 1 G. A. Somorjai, A. M. Contreras, M. Montano and R. M. Rioux, *Proc. Natl. Acad. Sci. U. S. A.*, 2006, **103**, 10577–10583.
- 2 A. T. Bell, *Science*, 2003, **299**, 1688–1691.
- 3 *Nanocatalysis*, ed. U. Heiz and U. Landman, Springer, Berlin, 2007.
- 4 A. R. Tao, S. Habas and P. Yang, *Small*, 2008, **4**, 310–325.
- 5 Y. Xia, Y. Xiong, B. Lim and S. E. Skrabalak, *Angew. Chem., Int. Ed.*, 2009, **48**, 60–103.
- 6 G. A. Somorjai, *Introduction to Surface Chemistry and Catalysis*, Wiley-Interscience, New York, 1994.
- 7 C. Burda, X. Chen, R. Narayanan and M. A. El-Sayed, *Chem. Rev.*, 2005, **105**, 1025–1102.
- 8 *Carbon Nanotubes: Synthesis, Structure, Properties, and Applications*, ed. M. S. Dresselhaus, G. Dresselhaus and P. Avouris, Springer, Berlin, 2000.
- 9 K. R. Chi, *Nat. Methods*, 2009, **6**, 15–18.
- 10 W. Xu, J. S. Kong, Y.-T. E. Yeh and P. Chen, *Nat. Mater.*, 2008, **7**, 992–996.
- 11 W. Xu, J. S. Kong and P. Chen, *J. Phys. Chem. C*, 2009, **113**, 2393–2404.
- 12 W. Xu, J. S. Kong and P. Chen, *Phys. Chem. Chem. Phys.*, 2009, **11**, 2767–2778.
- 13 X. Zhou, W. Xu, G. Liu, D. Panda and P. Chen, *J. Am. Chem. Soc.*, 2010, **132**, 138–146.
- 14 P. Chen, W. Xu, X. Zhou, D. Panda and A. Kalininskiy, *Chem. Phys. Lett.*, 2009, **470**, 151–157.
- 15 W. Xu, H. Shen, G. Liu and P. Chen, *Nano Res.*, 2009, **2**, 911–922.
- 16 W. Xu, H. Shen, Y. J. Kim, X. Zhou, G. Liu, J. Park and P. Chen, *Nano Lett.*, 2009, **9**, 3968–3973.
- 17 R. McCreery, *Chem. Rev.*, 2008, **108**, 2646–2687.
- 18 K. Gong, F. Du, Z. Xia, M. Durstock and L. Dai, *Science*, 2009, **323**, 760–764.
- 19 J. K. Campbell, L. Sun and R. M. Crooks, *J. Am. Chem. Soc.*, 1999, **121**, 3779–3780.
- 20 I. Heller, J. Kong, H. A. Heering, K. A. Williams, S. G. Lemay and C. Dekker, *Nano Lett.*, 2005, **5**, 137–142.

- 21 I. Heller, J. Kong, K. A. Williams, C. Dekker and S. G. Lemay, *J. Am. Chem. Soc.*, 2006, **128**, 7353–7359.
- 22 J. Zhang, X. Liu, R. Blume, A. Zhang, R. Schloegl and D. S. Su, *Science*, 2008, **322**, 73–77.
- 23 B. R. Goldsmith, J. G. Coroneus, A. A. Kane, G. A. Weiss and P. G. Collins, *Nano Lett.*, 2008, **8**, 189–194.
- 24 B. R. Goldsmith, J. G. Coroneus, V. R. Khalap, A. A. Kane, G. A. Weiss and P. G. Collins, *Science*, 2007, **315**, 77–81.
- 25 Y. Fan, B. R. Goldsmith and P. G. Collins, *Nat. Mater.*, 2005, **4**, 906–911.
- 26 R. E. Palacios, F.-R. F. Fan, A. J. Bard and P. F. Barbara, *J. Am. Chem. Soc.*, 2006, **128**, 9028–9029.
- 27 R. E. Palacios, F.-R. F. Fan, J. K. Grey, J. Suk, A. J. Bard and P. F. Barbara, *Nat. Mater.*, 2007, **6**, 680–685.
- 28 L. Edman, Z. FiSldes-Papp, S. Wennmalm and R. Rigler, *Chem. Phys.*, 1999, **247**, 11–22.
- 29 K. Velonia, O. Flomenbom, D. Loos, S. Masuo, M. Cotlet, Y. Engelborghs, J. Hofkens, A. E. Rowan, J. Klafter, R. J. M. Nolte and F. C. de Schryver, *Angew. Chem., Int. Ed.*, 2005, **44**, 560–564.
- 30 B. P. English, W. Min, A. M. van Oijen, K. T. Lee, G. Luo, Y. Sun, B. J. Cherayil, S. C. Kou and X. S. Xie, *Nat. Chem. Biol.*, 2006, **2**, 87–94.
- 31 R. D. Smiley and G. G. Hammes, *Chem. Rev.*, 2006, **106**, 3080–3094.
- 32 M. B. Roeffaers, B. F. Sels, H. Uji-i, F. C. De Schryver, P. A. Jacobss, D. E. De Vos and J. Hofkens, *Nature*, 2006, **439**, 572–575.
- 33 K. Naito, T. Tachikawa, M. Fujitsuka and T. Majima, *J. Phys. Chem. C*, 2008, **112**, 1048–1059.
- 34 S. Rosenblatt, Y. Yaish, J. Park, J. Gore, V. Sazonova and P. L. McEuen, *Nano Lett.*, 2002, **2**, 869–872.
- 35 R. S. Twigg, *Nature*, 1945, **155**, 401–402.
- 36 H. Huang, R. Maruyama, K. Noda, H. Kajiura and K. Kadono, *J. Phys. Chem. B*, 2006, **110**, 7316–7320.
- 37 E. Betzig, G. H. Patterson, R. Sougrat, O. W. Lindwasser, S. Olenych, J. S. Bonifacino, M. W. Davidson, J. Lippincott-Schwartz and H. F. Hess, *Science*, 2006, **313**, 1642–1645.
- 38 M. J. Rust, M. Bates and X. Zhuang, *Nat. Methods*, 2006, **3**, 793–796.
- 39 S. T. Hess, T. P. K. Girirajan and M. D. Mason, *Biophys. J.*, 2006, **91**, 4258–4272.
- 40 M. Bates, B. Huang and X. Zhuang, *Curr. Opin. Chem. Biol.*, 2008, **12**, 505–514.
- 41 M. Bates, B. Huang, G. T. Dempsey and X. Zhuang, *Science*, 2007, **317**, 1749–1753.
- 42 B. Huang, W. Wang, M. Bates and X. Zhuang, *Science*, 2008, **319**, 810–813.
- 43 R. E. Thompson, D. R. Larson and W. W. Webb, *Biophys. J.*, 2002, **82**, 2775–2783.
- 44 A. Yildiz, J. N. Forkey, S. A. McKinney, T. Ha, Y. E. Goldman and P. R. Selvin, *Science*, 2003, **300**, 2061–2065.
- 45 A. J. Bard and L. R. Faulkner, *Electrochemical Methods: Fundamentals and Applications*, John Wiley & Sons, Inc., 2000.
- 46 S. Banerjee, T. Hemraj-Benny and S. S. Wong, *Adv. Mater.*, 2005, **17**, 17–29.
- 47 A. Hirsch, *Angew. Chem., Int. Ed.*, 2002, **41**, 1853–1859.
- 48 P. L. McEuen, *Phys. World*, 2000, **13**, 31–36.
- 49 H. Dai, *Acc. Chem. Res.*, 2002, **35**, 1035–1044.
- 50 M. Y. Sfeir, F. Wang, L. M. Huang, C. C. Chuang, J. Hone, S. P. O'Brien, T. F. Heinz and L. E. Brus, *Science*, 2004, **306**, 1540–1543.
- 51 N. S. Lewis, *J. Phys. Chem. B*, 1998, **102**, 4843–4855.
- 52 H. Gerischer, in *Physical Chemistry An Advanced Treatise*, ed. H. Eyring, Academic Press, New York/London, 1970, vol. IXA.
- 53 C. E. D. Chidsey, *Science*, 1991, **251**, 919–922.
- 54 J. U. Lee, *Appl. Phys. Lett.*, 2005, **87**, 073101.
- 55 P. Avouris, M. Freitag and V. Perebeinos, *Nat. Photonics*, 2008, **2**, 341–350.
- 56 N. M. Gabor, Z. Zhong, K. Bosnick, J. Park and P. L. McEuen, *Science*, 2009, **325**, 1367–1371.
- 57 A. J. Bard and F.-R. F. Fan, *Acc. Chem. Res.*, 1996, **29**, 572–578.
- 58 A. J. Bard, *ACS Nano*, 2008, **2**, 2437–2440.
- 59 R. W. Murray, *Chem. Rev.*, 2008, **108**, 2688–2720.
- 60 C. Lei, D. Hu and E. J. Ackerman, *Chem. Commun.*, 2008, 5490–5492.
- 61 C. Lei, D. Hu and E. Ackerman, *Nano Lett.*, 2009, **9**, 655–658.
- 62 T. Tachikawa and T. Majima, *J. Am. Chem. Soc.*, 2009, **131**, 8485–8495.
- 63 F.-R. F. Fan and A. J. Bard, *Nano Lett.*, 2008, **8**, 1746–1749.
- 64 M. M. Collinson and R. M. Wightman, *Science*, 1995, **268**, 1883–1885.
- 65 Y.-L. Chang, R. E. Palacios, F.-R. F. Fan, A. J. Bard and P. F. Barbara, *J. Am. Chem. Soc.*, 2008, **130**, 8906–8907.